A Cascade-Formed Accurate Quasi-PR Controller Realization by Pole-Zero Placement

Chao GAO, Shuyu ZHANG, Bo LU, Wenlong DING, Ka Nang LEUNG, and Poh Chiang LOH

***Abstract*—PR controller has been widely researched in various control systems for its robustness and simplicity. However, a traditional PR controller with relatively small integral gain, used for higher-order harmonics to keep stability, will cause increases in magnitudes, and decreases in phase around resonant frequency, and jeopardize stability. These all call for a more precise realization of PR controller. This paper proposes a cascade-formed PR controller realization method, which proves to realize PR controller more accurately even with a relatively small integral gain. The method is to decompose a PR controller into multiple independent PR units, and each PR unit is realized by mapping PR controller's parameters to its pole and zero positions. The distance between a pole-zero pair is found related to frequency characteristic error and is restricted accordingly to limit the error. Comprehensive comparisons of PR controllers realized by cascade form and the traditional parallel form have been conducted theoretically and experimentally, verifying that the cascade realization method is more accurate.**

***Index Terms*—Cascade form, pole-zero placement, PR controller, realization.**

I. Introduction

In recent decades, proportional resonant (PR) controllers have attracted increasing research attention [1], especially in power electronics such as motor drives [2], active power filters [3], grid-tied inverters with LCL filter [4], and so on, for its excellent robustness and simplicity [5], [6].

Traditionally, PR controllers are realized by parallel form, i.e., the parallel of a proportional (P) controller and one or multiple resonant (R) controllers [7]. R controller is derived initially from transforming synchronous frame proportional integrator (PI) controller into the stationary frame for integrating sinusoidal signal [2], [8]. Thus, the ideal R controller is also called general integrator (GI) [9] or sinusoidal signal integrator (SSI) [10] with infinite gain at its resonant frequency and a relatively small gain at other frequencies. The parallel of multiple R controllers provides infinite gain at multiple resonant frequencies, and thus zero tracking error for those frequencies is guaranteed [11]. Further, with the P controller added to R controllers, higher gain at frequencies other than resonant frequencies is obtained, broadening bandwidth [12]. Since any finite value is trivial when added to an infinite value, a parallel-formed ideal PR controller can maintain its frequency characteristics at a resonant frequency the same as that of the corresponding R controller. Therefore, the infinite gain of the R controller is the prerequisite of the accurate realization of the parallel-formed PR controller.

In practice, the usage of a damped PR (quasi-PR) controller, whose resonant peak is finite, is recommended for several reasons. First, an ideal PR controller acts like an infinite quality factor network and is unrealizable [13], [14]. Besides, [8], [15] find quasi-PR controller is less sensitive to fundamental frequency deviation because of the broader bandwidth of its resonant peaks. Meanwhile, its phase changes slower around resonant frequencies [16] alleviating the anomalous peaks of the closed-loop transfer function that incorporates a PR controller [17], [18]. Thus, a quasi-PR controller is widely used.

There are multiple ways to design a PR controller [19]–[21]. However, none of these design methods consider the deviation of frequency characteristic caused by replacing ideal R controller with damped R controller. The situation exacerbates with resonant frequency increasing. Multiple application needs PR controller to be tuned at relatively high frequency. For example, an active power filter (APF) usually needs a PR controller to be tuned at up to 13th order harmonic [22] to compensate the corresponding harmonic. More critically, when APF is used to filter switching harmonics [23], the resonant frequency of PR controller should be tuned at thousands of Hertz. Similarly, when a PR controller is applied to the motor drive to suppress torque ripple caused by distorted back electromotive force, it also needs to be tuned at $6np$ ($n \in \mathbf{Z}$) times mechanical angle speed where p is the number of pole pairs [24]. It is found that the integral gain must decrease with resonant frequency increasing to keep stability [25], [26], and lead to more error on frequency characteristics. Reference [26] proposes an iteration algorithm to correct the errors of

Manuscript received June 6, 2023; revised August 30, 2023; accepted October 25, 2023. Date of publication March 30, 2024; date of current version November 1, 2023. This work was supported in part by the National Natural Science Foundation of China under Grant 62203275, in part by Shandong Province Science Fund for Excellent Young Scientists Found Program under Grant 2022HYYQ-022, and in part by National Key R&D Plan of China under Grant 2022YFF0712700. *(Corresponding author: Wenlong Ding.)*

C. Gao, K. N. Leung, and P. C. Loh are with the Department of Electronic Engineering, the Chinese University of Hong Kong, Hong Kong, China (e-mail: chaogao@link.cuhk.edu.hk; knleung@ee.cuhk.edu.hk; pcloh@ee.cuhk.edu.hk).

S. Zhang is with the School of Engineering, Stanford University, Stanford, CA 94305, United States (e-mail: mojisama0@gmail.com).

B. Lu is with the Academy for Engineering and Technology, Fudan University, Shanghai 200433, China (e-mail: 2453708227@qq.com).

W. Ding is with the School of Control Science and Engineering, Shandong University, Jinan 250100, China (e-mail: dingwl8804@163.com).

Digital Object Identifier 10.24295/CPSSTPEA.2023.00046

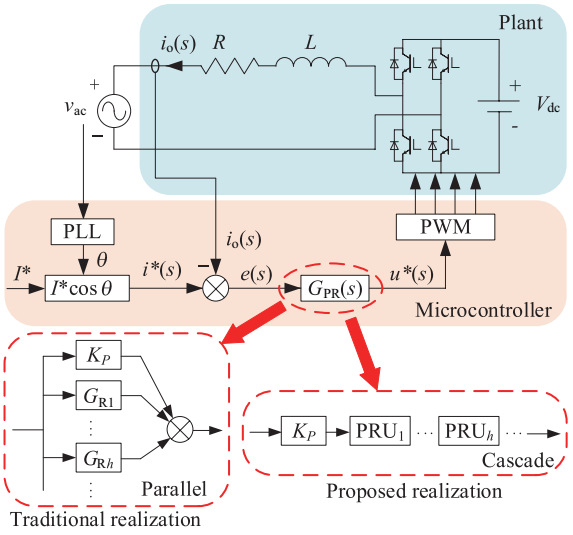

Fig. 1. Schematic diagram of L-filtered grid-tied converter.

phases, which takes a large amount of calculation and does not consider the magnitude errors.

In this paper, the inaccuracy of the parallel realization of the quasi-PR controller is first demonstrated and will be tackled by a new cascade realization form, which more accurately realizes the magnitudes and phases of quasi-PR controller at resonant frequencies. Since this paper deals with only quasi-PR controllers rather than ideal PR controllers, in the following parts, the prefix "quasi-" will be saved for conciseness, and the words "PR or R controller" refer to the quasi-PR or quasi-R controller.

This paper is organized as follows. In Section II, the inaccuracy of the PR controller's parallel realization is demonstrated. In Section III, the PR controller's pole-zero distribution characteristics and resonant decoupling property are formulated, based on which a cascade realization method for PR controller is proposed. Section IV presents the relevant experimental results and analysis, followed by Section V, the conclusion.

II. Realization Error Analysis of Parallel PR Controller

Since this paper only focuses on the new PR controller realization method, we use a commonly used L-filtered grid-tied converter to illustrate the performance of the controller without excluding the possibility of other application situations. The schematic diagram of the grid-tied converter with its controller is shown in Fig. 1, where L and R are the inductance and parasitic resistance of the L filter, respectively, $i_o(s)$ is the output current, $i^*(s)$ is the reference current, $e(s)$ is the error signal, $G_{PR}(s)$ is the PR controller which is traditionally realized by the parallel form. The transfer function from reference voltage, $u_{ref}(s)$, to output current, $i_o(s)$, is:

$$P(s) = \frac{i_o(s)}{u_{ref}(s)} = \frac{e^{-1.5sT}}{sL+R} \tag{1}$$

TABLE I
Relevant Parameters of the PR Controller and the System

Symbol	Description	Value
L	L filter inductance	5 mH
R	L filter resistance	0.15 Ω
f_1	Grid fundamental frequency	50 Hz
V_g	Grid voltage (RMS)	220 V
V_{dc}	DC-link voltage	700 V
f_s	Sampling frequency	5 kHz
f_{sw}	Switching frequency	5 kHz
K_p	Proportional gain	15.7
ω_{ch}	Resonant cutoff frequency	1

where T is the sampling period, and $e^{-1.5sT}$ represents the 1.5 sampling delay introduced by digital computation and PWM.

A conventional parallel PR controller can be expressed as:

$$G_{PR}(s) = K_P + \sum_h G_{Rh}(s) \tag{2}$$

where K_P is the proportional gain, and $G_{Rh}(s)$ is the R controller tuned at h order harmonic, which can be expressed as:

$$G_{Rh}(s) = K_{Ih}\frac{2\omega_{ch}[s\cos(\varphi_h) - h\omega_1\sin(\varphi_h)]}{s^2 + 2\omega_{ch}s + h^2\omega_1^2} \tag{3}$$

where K_{Ih} is the integral gain, i.e., the resonant magnitude of $G_{Rh}(s)$, and ideally it should also be the resonant magnitude of $G_{PR}(s)$, ω_{ch} is the resonant cutoff frequency, φ_h is the phase lead of $G_{Rh}(s)$, and is also expected to be the phase of $G_{PR}(s)$ at the corresponding resonant frequency, $h\omega_1$. By solving the denominator of (3), the poles of the PR controller are given by:

$$s_{1,2} = -\omega_{ch} \pm j\sqrt{h^2\omega_1^2 - \omega_{ch}^2} \tag{4}$$

At frequencies other than resonant frequencies, the PR controller can be regarded as a proportional controller, and all R controllers can be neglected. Thus, K_P decides the bandwidth of the controller with the following relationship:

$$K_p = \alpha_c L \tag{5}$$

where α_c is the bandwidth of the controller and usually set to $\omega_s/10$ (ω_s represents the sampling angle frequency). With parameters listed in Table I, K_P is calculated as 15.7. Phase lead is used to compensate for the 1.5 sampling delay [26], and improve phase margin, i.e.,

$$\varphi_h = 1.5 \times 2\pi f_1 hT \tag{6}$$

where f_1 is the grid fundamental frequency.

K_{Ih} can be approximated as the resonant magnitude [16]. Thus, it should be set high enough for a small tracking error [16]. Meanwhile, at high frequencies, a high K_{Ih} may critically reduce the stability margin and response speed [25], [26]. Thus, the tuning of K_{Ih} differs in resonant frequency and should strike a balance between small steady-state error and good stability.

A parallel PR controller tuned at $h \in \{1,3,5,\ldots,19\}$ order harmonics is realized aiming to resist grid voltage harmonics

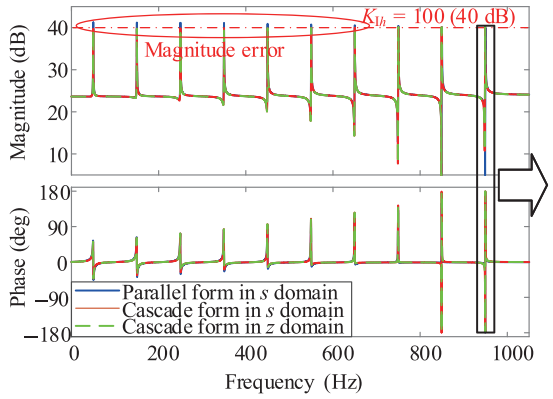

(a)

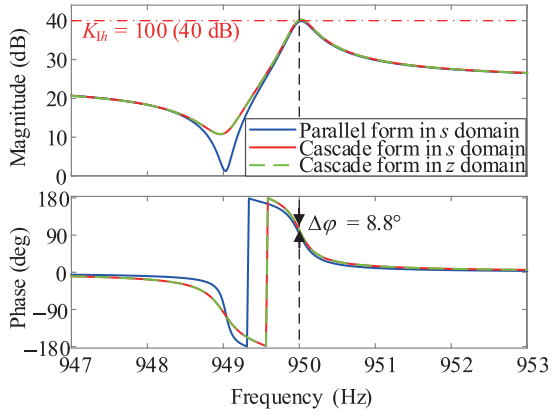

(b)

Fig. 2. Bode plots of PR controllers of parallel form in *s* domain, cascade form in *s* domain and cascade form in *z* domain, with K_{Ih} set to 100, $h \in \{1,3,\ldots,19\}$ and other parameters listed in Table I. (a) full view. (b) zoom-in view of black box in the full view.

TABLE II
MAGNITUDES AND PHASES OF PARALLEL PR CONTROLLER AT RESONANT FREQUENCIES

Harmonic order, h	1	3	17	19
Ideal magnitude, K_{Ih}	100	100	100	100
Real magnitude, M_{PRh}	115.2	114.7	100.5	97.5
Magnitude error	15.2	14.7	0.5	−2.5
Ideal phase, φ_h	5.4°	16.2°	91.8°	102.6°
Real phase, φ_{PRh}	4.8°	14.0°	82.7°	93.4°
Phase error	−0.6°	−2.2°	−9.1°	−9.2°

at those frequencies. K_{Ih} is set to 100, and other parameters can be found in Table I. The Bode plot of the parallel PR controller is depicted in Fig. 2. It can be obviously found that at lower resonant frequencies, the resonant magnitudes exceed K_{Ih} (100 or 40 dB), which is circled in red. For clearer investigation Table II lists the expected resonant magnitude (K_{Ih}), and phase lead (φ_h), and actual values of the resultant parallel PR controller (M_{PRh}, φ_{PRh}) at selected 1st, 3rd, 17th, and 19th order harmonics to see its characteristics at low and high frequency. It can be found that the resonant magnitude and phase of parallel PR controller deviates from the expected value a lot. PR controller's magnitude, M_{PRh}, exceeds K_{Ih} by up to 15.2 at

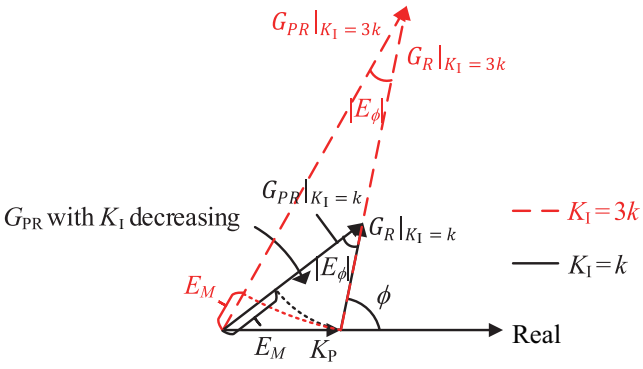

Fig. 3. Schematic diagram for illustrating phase and magnitude error caused by parallel realization with K_I varying.

h = 1. PR controller's phase, φ_{PRh}, lags φ_h by about 9.2° at h = 19, and this may jeopardize stability.

Fig. 3 illustrates the magnitude error and phase error of a PR controller at resonant frequency. Each vector represents a complex value of either an R controller, or a P controller, or their summation, the PR controller. The K_I of $G_R(s)$ or $G_{PR}(s)$ in dashed red line is higher than that of $G_R(s)$ or $G_{PR}(s)$ in solid black line. Phase error, $E_\varphi = \angle G_{PR}(s) - \angle G_R(s)$, is the angle between $G_{PR}(s)$ and $G_R(s)$, as marked in Fig. 3. It can be seen that $|E_\varphi|$ increase as K_I decreases. On the other hand, magnitude error, E_M, is the difference between $|G_{PR}|$ and $|G_R|$, which is obtained graphically by drawing a circle (dotted line) centered at the endpoint of $G_{PR}(s)$ with a radius of K_I. Obviously, $|E_M|$ also increase as K_I decreases. Thus, for high-order harmonics where K_{Ih} is set small, the traditional parallel realization will result in a relatively significant increase in magnitude and decrease in phase. A new realization form is proposed to tackle this problem in the following section.

III. Cascade Realization of PR Controller Using Pole-Zero Placement

In the analysis of the parallel PR controller (addition form), we always try to ignore the smaller part in the summation, which needs to be more accurate. In the analysis of the transfer function in cascade form (multiplication form), the synthesized frequency characteristics will be the exact the summation of all frequency characteristics of multiplier transfer functions since $\angle G_1G_2 = \angle G_1 + \angle G_2$, and $20\log|G_1G_2| = 20\log|G_1| + 20\log|G_2|$. Thus, in this section, we try to analyze the PR controller in cascade form and find ways to realize a PR controller directly in cascade form.

A. Pole-Zero Analysis of PR Controller in Cascade Form

Fig. 4 shows a typical pole-zero map of a PR controller tuned at only two resonant frequencies, ω_1 and $3\omega_1$. It can be found that poles are located around $\pm jh\omega_1$ as specified by (4). Zeros are extremely close to their corresponding poles with respect to other poles (note the scale of the real and imaginary axes). In fact, it is a common characteristic of PR controller's

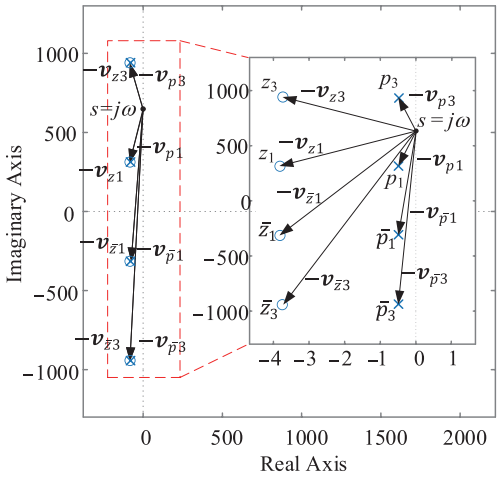

Fig. 4. Pole-zero map of PR controller whit $h \in \{1,3\}$, $K_{ih} = 100$ for all h. Other parameters are listed in Table I.

pole-zero map that poles and zeros are located closely in pairs around resonant frequencies. Thus, a PR controller can be expressed as:

$$G_{\mathrm{PR}}(s) = K_{\mathrm{P}} \prod_i \frac{s - z_i}{s - p_i} \tag{7}$$

where z_i and p_i are a pair of zero and pole tuned at the same frequency.

According to (7), the frequency characteristics of the PR controller at ω will be:

$$G_{\mathrm{PR}}(j\omega) = K_{\mathrm{P}} \frac{(j\omega - z_1)(j\omega - z_3)(j\omega - \bar{z}_1)(j\omega - \bar{z}_3)}{(j\omega - p_1)(j\omega - p_3)(j\omega - \bar{p}_1)(j\omega - \bar{p}_3)} \tag{8}$$

where $\bar{x}$ means the conjugate value of x. All poles and zeros can be calculated by simply setting the denominator or numerator of (2) to 0. The difference between $s = j\omega$ and a pole or zero is denoted as a vector, v_x, $x \in$ {poles, zeros}. For clarity, $-v_x$ is shown in Fig. 4 with the reverse direction of v_x. Therefore, (8) becomes:

$$G(j\omega) = K_{\mathrm{P}} \frac{v_{z1} v_{z3} v_{\bar{z}1} v_{\bar{z}3}}{v_{p1} v_{p3} v_{\bar{p}1} v_{\bar{p}3}} \tag{9}$$

When $s = j\omega$ is at the position (see Fig. 4) far away from all poles and zeros (with respect to the distance within a pole-zero pair), a pair of pole and zero can be regarded as overlapping, and v_{zx}/v_{px} is approximated to 1, where z_x and p_x are a pair of zero and pole. Then, $G_{\mathrm{PR}}(j\omega)$ is approximated to:

$$G_{\mathrm{PR}}(j\omega) \approx K_{\mathrm{P}} \tag{10}$$

For example, $j2\omega_1$ is far away from the resonant frequency, $j\omega_1$ and $j3\omega_1$ where poles and zeros are located. And $K_{\mathrm{P}} = 15.7$ is highly close to the actual value $G_{\mathrm{PR}}(j2\omega_1) = 15.62\angle -0.65°$ confirming the accuracy of the approximation (10).

Moreover, if s is close to a pole-zero pair, the assumption of $v_{zx}/v_{px} \approx 1$ for that pole-zero pair will not hold, and (9) will be approximated to:

$$G_{\mathrm{PR}}(j\omega) \approx K_{\mathrm{P}} \frac{v_{zx}}{v_{px}} = K_{\mathrm{P}} \frac{j\omega - z_x}{j\omega - p_x} \tag{11}$$

For example, when $s = j\omega_1$, (11) becomes:

$$G_{\mathrm{PR}}(j\omega_1) \approx K_{\mathrm{P}} \frac{j\omega_1 - z_1}{j\omega_1 - p_1} = 116.2\angle 5.01° \tag{12}$$

which is very close to the actual value, $G_{\mathrm{PR}}(j\omega_1) = 115.58 \angle 4.7°$ confirming the accuracy of the approximation (11).

To summarize, (10) and (11) effectively approximate PR controller's frequency characteristics. When considering frequency far from resonant frequencies, poles and zeros align, PR controller is simplified to K_{P}, i.e., (10). When considering frequency near a resonant frequency, the corresponding pole-zero pair dominate, simplifying the PR controller to $K_{\mathrm{P}}(s-z)/(s-p)$, i.e., (11). Thus, $(s-z)/(s-p)$ can be regarded as a PR controller unit (PRU) determining a resonant peak, and (7) can be rewritten as:

$$G_{\mathrm{PR}}(s) = K_{\mathrm{P}} \prod \mathrm{PRU} \tag{13}$$

In real-coefficient PR controller, PRUs always appear in conjugate pairs. Each PRU, represented as $(s - z_h)/(s - p_h)$, and its conjugate, $(s - \bar{z}_h)/(s - \bar{p}_h)$, regulate the positive and negative sequences, respectively. If the conjugate PRU is not used, only the positive or negative sequence will be regulated resulting in a reduced order generalized integrator (ROGI) [27].

This property of the PR controller, termed "resonant decoupling" in this paper, offers insights, and allows one to realize the frequency characteristics of a PR controller by cascading individual PRUs, as depicted in Fig. 1. This concept will be detailed in the following subsections. In the next subsection, a detailed examination of the resonant decoupling property will be conducted, and the errors associated with its application are assessed.

B. Applicability of Resonant Decoupling Property

The reason that omitting a pole-zero pair will cause difference on frequency characteristics is that the pole and zero do not align precisely. Consider a pole-zero pair: the zero, $z_k = r_z + j\omega_z$, and the pole, $p_k = r_p + j\omega_p$, resonant at $\omega_p = k\omega_1 \approx \omega_z$. According to (7), the phase at the frequency ω, which is far away from ω_{p}, can be expressed as

$$\angle G_{\mathrm{PR}}(j\omega) = \sum_{i \neq k} \angle \frac{j\omega - z_i}{j\omega - p_i} + \angle \frac{j\omega - z_k}{j\omega - p_k} = \varphi^* + \triangle\varphi_k \tag{14}$$

where φ^* denotes the phase $\angle G_{\mathrm{PR}}(j\omega)$ with pole-zero pair (p_k, z_k), omitted, and $\Delta\varphi_k$ denotes the phase variation caused by (p_k, z_k). When resonant decoupling property is implemented, the pole-zero pair (p_k, z_k), is omitted, and therefore, a phase error, $-\Delta\varphi_k$, will be caused on frequency characteristics at ω. As shown in Fig. 5, $\Delta\varphi_k$ is the angle formed by two vectors $(s - z_k)$ and $(s - p_k)$. γ_p and γ_z are relatively small and can be approximated by their tangent values, which yields

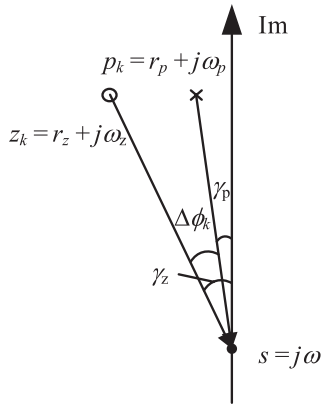

Fig. 5. Schematic pole-zero map of PR controller.

$$\begin{aligned}\triangle\varphi_k &= \gamma_z - \gamma_p \approx \tan(\gamma_z) - \tan(\gamma_p) \\ &= \frac{|r_z|}{\omega - \omega_z} - \frac{|r_p|}{\omega - \omega_p} \approx \frac{r_p - r_z}{\omega - \omega_p}\end{aligned} \tag{15}$$

(15) indicates that $\Delta\varphi_k$ is in proportion to $(r_p - r_z)$ and in inverse proportion to $(\omega - \omega_p)$. Fig. 6(a) shows the relationship between the absolute phase variation, $|\Delta\varphi_k|$, and $|\text{Real}(z_k - p_k)|$ and $|\omega - \omega_p|$ graphically.

So, the difference between the real parts of a pole-zero pair, $\text{Real}(z_k - p_k) = (r_p - r_z)$, should be restricted so that the phase error, $-\Delta\varphi_k$, is acceptable. The maximum allowable phase draft can be uniformly set to ±0.02 rad (±1.15°) at resonant frequency, $h\omega_1$, for all h, i.e.

$$\left|\triangle\varphi_k\right| = \left|\frac{\text{Real}(z_k - p_k)}{h\omega_1 - k\omega_1}\right| < 0.02 \tag{16}$$

Consequently

$$-0.02\min\triangle\omega < \text{Real}(z_k - p_k) < 0.02\min\triangle\omega \tag{17}$$

where $\min\Delta\omega = \min|h-k|\omega_1$. Usually, resonant frequencies are set first, i.e., the min $\Delta\omega$ is known. Thus, (17) restricts the real part of the zeros.

On the other hand, the magnitude of G_{PR} (s) at ω is

$$\left|G_{\text{PR}}(j\omega)\right| = K_{\text{p}} \prod_{j \neq k} \left|\frac{j\omega - z_j}{j\omega - pj}\right| \cdot \left|\frac{j\omega - z_k}{j\omega - p_k}\right| \tag{18}$$

where the factor $K_{\text{p}} \prod_{j\neq k} \left|\frac{j\omega - z_j}{j\omega - pj}\right|$ denoted as M^* is the magnitude $|G_{\text{PR}}(j\omega)|$ with pole-zero pair, (p_k, z_k), omitted. As for another part

$$\left|\frac{j\omega - z_k}{j\omega - p_k}\right| = \left|\frac{r_z + j(\omega_z - \omega)}{r_p + j(\omega_p - \omega)}\right| \tag{19}$$

when ω is far away from ω_p, r_z and r_p are far smaller than $|\omega_p - \omega|$, or $|\omega_z - \omega|$, they can be neglected, and the magnitude of G_{PR} $(j\omega)$ is approximated to

$$\left|G_{\text{PR}}(\omega)\right| \approx M^* \left|\frac{\omega_z - \omega}{\omega_p - \omega}\right| = M^* \left(1 + \frac{\omega_z - \omega_p}{\omega_p - \omega}\right) \tag{20}$$

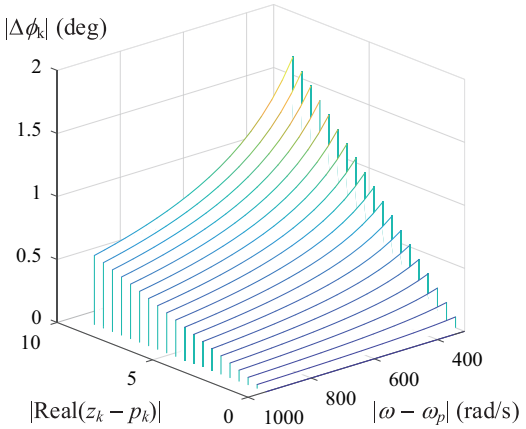

(a)

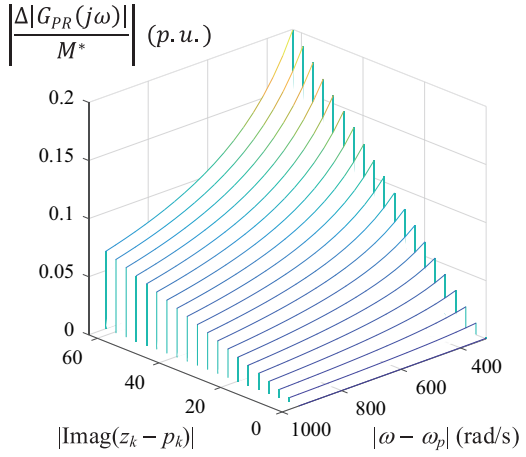

(b)

Fig. 6. (a) phase error and (b) magnitude error with $\text{Real}(z_k - p_k)$ or $\text{Imag}(z_k - p_k)$ and $|\omega - \omega_k|$ varying.

Then the variation in the magnitude of G_{PR} $(j\omega)$ is

$$\triangle\left|G_{\text{PR}}(j\omega)\right| = \left|G_{\text{PR}}(j\omega)\right| - M^* = M^* \frac{\omega_z - \omega_p}{\omega_p - \omega} \tag{21}$$

which means the variation of the magnitude, $\Delta|G_{\text{PR}}(j\omega)|$, is in proportion to M^* and a factor $(\omega_z - \omega_p)/(\omega_p - \omega)$, which is introduced by a pole-zero pair, (p_k, z_k), tuned at $k\omega_1$. Fig. 6(b) illustrates the relationship between the absolute magnitude variation in per unit, $\left|\frac{\triangle|G_{\text{PR}}(jh\omega_1)|}{M^*}\right|$, and the variations in $|\text{Imag}(z_k - p_k)|$ and $|\omega - \omega_p|$.

The bias of the imaginary part of a zero, $\text{Imag}(z_k - p_k) = (\omega_z - \omega_p)$, should be restricted such that the omitted pole-zero pair does not affect the magnitudes of other resonant frequencies too much. The maximum allowable deviation ratio of $|G_{\text{PR}}(j\omega)|$ can be set uniformly to 2% at resonant frequency, $h\omega_1$, for all h, i.e.

$$\left|\frac{\triangle|G_{\text{PR}}(jh\omega_1)|}{M^*}\right| = \left|\frac{\text{Imag}(z_k - p_k)}{k\omega_1 - h\omega_1}\right| < 2\% \tag{22}$$

Then

$$-0.02\min\triangle\omega < \mathrm{Imag}(z_k - p_k) < 0.02\min\triangle\omega \tag{23}$$

(17) and (23) restrict zeros within squares centered at their paired poles. In this way, the maximum effect by omitting a pole-zero pair to frequency characteristics at other resonant frequencies is limited to ±2% magnitude error and ±0.02 rad phase error. However, note that when omitting multiple pole-zero pairs, the error will be superimposed, and may exceed the abovementioned limit. But this should not be a worry since (17) and (23) use min $\Delta\omega$, which corresponds to the adjacent pole-zero pair to be omitted. As for further pole-zero pair, its distance to the frequency of concern is much larger, and the influence will be small enough to be omitted.

C. Cascade Realization of PR Controller in the s Domain

The problem that paralleling scheme fails to realize the PR controller accurately will be tackled by cascade realization in this subsection, which can realize the PR controller more accurately.

A PR controller can be solely determined by K_P, $K_{\mathrm{I}h}$, φ_h, and ω_{ch}, provided that $h\in H$ and resonant frequencies $h\omega_1$ are known. Those parameters appear explicitly in the expressions of parallel-formed PR controllers (2) and (3), and should be tuned directly by traditional design methods as summarized in Section II. However, these parameters do not explicitly show in the expression of cascade-formed PR controller (7), except for K_P. Thus, by mapping all those parameters to the locations of poles and zeros, a cascade realization of a PR controller can be done.

The location of a pole can be obtained directly since their imaginary part is the resonant frequency $h\omega_1$ [18], and its real part is $-\omega_{ch}$ according to (4).

The locations of zeros are determined by desired frequency characteristics around resonant frequencies. According to the resonance-decoupling property of PR controller, the frequency response around a particular resonant frequency $k\omega_1$ can be approximated by

$$G_{\mathrm{PR}}(s) \approx K_\mathrm{p}\frac{s - z_k}{s - p_k} \tag{24}$$

where $p_k = -\omega_{ck} + jk\omega_1$, $z_k = r_k + j\omega_k$. The magnitude of $G_{\mathrm{PR}}(s)$ approaches its maximum at resonant point, $s = jk\omega_1$, which should be the integral gain $K_{\mathrm{I}k}$, i.e.

$$K_{\mathrm{I}k} = K_\mathrm{p}\left|\frac{jk\omega_1 - z_k}{jk\omega_1 - p_k}\right| \tag{25}$$

namely

$$\left|jk\omega_1 - z_\mathrm{k}\right| = \frac{K_{\mathrm{I}k}\omega_{ck}}{K_\mathrm{p}} \tag{26}$$

which defines a trajectory of z_k, a circle centered at $jk\omega_1$ with a radius of $K_{\mathrm{I}k}\,\omega_{ck}/K_\mathrm{P}$ (see blue line in Fig. 7). In addition, the phase at the resonant frequency, $k\omega_1$, should be φ_k:

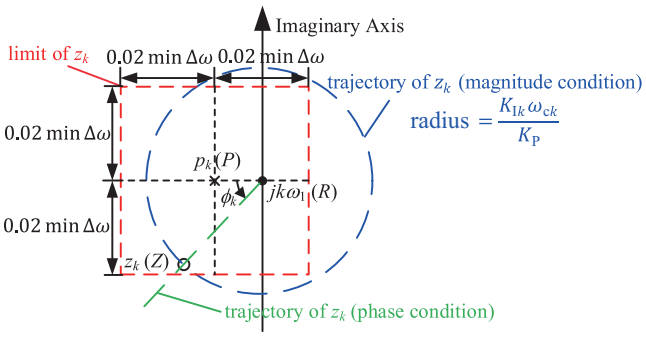

Fig. 7. Schematic pole-zero map around a pole-zero pair for illustrating the determination of z_k and its limit.

$$\varphi_k = \angle G_{\mathrm{PR}}(jk\omega_1) \approx \angle\left(\frac{z_k - jk\omega_1}{p_k - jk\omega_1}\right) \tag{27}$$

$\angle\left(\frac{z_k - jk\omega_1}{p_k - jk\omega_1}\right)$ is the angle $\angle$ZRP as shown in Fig. 7. Thus, z_k is located on the half-line starting from $jk\omega_1$ and form an angle φ_k counterclockwise with $(p_k - jk\omega_1)$ (see green line in Fig. 7). Combining the magnitude and phase conditions together, z_k is at the intersection of the circle (26) and the half-line (27). For now, a pair of pole and zero are located, namely a PRU, $(s - z_k)/(s - p_k)$ is determined. The conjugate PRU, $(s - \bar{z}_k)/(s - \bar{p}_k)$, can be obtained immediately if needed. By repeating the above steps, other PRUs tuned at other frequencies can be realized. Finally, the PR controller is obtained by cascading all PRUs and a K_P in the form of (7) or (13). From the standpoint of how subordinate controllers are linked, this proposed implementation method connects PRUs in a cascading manner differing from the conventional approach where P controllers and R controllers are connected in parallel. Therefore, this implementation can be seen as a dual form of the traditional parallel setup. It's worth noting that the PRU doesn't necessarily have to function as a PR controller. It can also be designed as a notch filter to block signals at a specific frequency. An ideal notch filter exhibits zero magnitude at its resonant frequency, meaning $K_{\mathrm{I}k} = 0$ and $z_k = jk\omega_1$.

In the previous subsection, how a zero should stay within a square region centered on its paired pole, with both sides measuring $0.04\min\Delta\omega$ (as illustrated by the red line in Fig. 7) is discussed. To maintain both magnitude and phase unchanged, this condition can be met by adjusting ω_{ch}. According to the magnitude condition (26), the location of the zero is also related to ω_{ch}. With $K_{\mathrm{I}h}$ set to 100, $h \in \{1,3,\ldots,19\}$ and other parameters listed in Table I, the maximal values for ω_{ch} for all h are obtained (the minimal values are zero). The minimum of these maximum values of ω_{ch} is calculated to be 0.95 justifying the suitability of the value 1 assigned to ω_{ch} in Section II.

D. Cascade Realization of PR Controller in the z Domain

Since controllers are all discrete for digital implementation, we ultimately need to obtain a PR controller in the z domain. Conventional discretization method for PR controller is

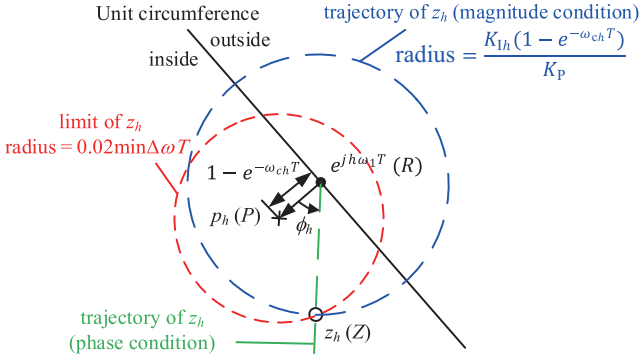

Fig. 8. Schematic pole-zero map for illustrating cascade PR controller realization in the *z* domain.

Tustin with prewarping, which discretizes PR controllers by discretizing each R controller first and then paralleling them. This inherently suits parallel-formed PR controller. If cascade-formed PR controller adopts Tustin with prewarping to discretize, it has to be decomposed into partial-fraction form or parallel form. That would be laborious. Considering this aspect, the cascade realization of PR controller in z domain will be elaborated in this subsection, which can be done directly without the prior *s* domain realization.

As concluded in the *s* domain, the pole-zero-gain form of a discrete PR controller is:

$$G_{\mathrm{PR}}(z) = K_{\mathrm{p}} \prod_i \frac{z - z_i}{z - p_i} \tag{28}$$

where z_i and p_i are a pair of zero and pole tuned at the same frequency. The frequency response of (28) can be obtained by substituting z with $e^{j\omega T}$, symmetrically to the *s* domain where *s* is substituted by $j\omega$. Geometrically this means z varies along the unit circle versus *s* along the imaginary axis. Thus, all the above analyses in the *s* domain can be applied to the *z* domain with a bit of adaptation.

Firstly, the pole should be placed at $e^{-\omega_{ch}T + jh\omega_1 T}$, corresponding to $p_h = -\omega_{ch} + jh\omega_1$ in the *s* domain. Secondly, when z is located around $e^{jh\omega_1 T}$, the circumference can be approximated by a straight line, and similarly, the angle $\angle$ZRP should be φ_h (see Fig. 8), to make sure accurate phase lead. Thirdly, the ratio $|z - z_h|/|z - p_h|$ should be equal to K_{Ih}/K_P, which determines a circular trajectory of z_h centered at $e^{jh\omega_1 T}$ with a radius of $K_{Ih}(1 - e^{jh\omega_1 T})/K_{\mathrm{p}}$ as shown in Fig. 8. Since z_h is located on the circle and the half line at the same time, z_h is obtained. The conjugate PRU can be obtained immediately, by $(z - \bar{z}_h)/(z - \bar{p}_h)$ if needed. Repeating the above steps gives other PRUs. And the final PR controller is realized by cascading all PRUs and K_{p} as (28).

Similarly, if the PRU is designed as a notch filter, K_{Ih} should be 0, and z_h should be $e^{jh\omega_1 T}$. Again, the distance between the pole and the zero should be restricted so as not to influence frequency characteristics in the distance. In *s* domain, all poles and zeros are distributed along the imaginary axis, and the effect of zero's movement can be separated into tangential and normal directions. Whereas in *z* domain, such a situation no longer exists, tangential direction toward a pair of pole and zero may not be tangential anymore for another pole-zero pair. Therefore, the limit of zero is set instead as a circle centered at the pole with a radius of $0.02\min\Delta\omega T$ (see Fig. 8). With parameters in Table I, K_{Ih} set to 100 and $h \in \{1,3,\ldots,19\}$, the maximal values for ω_{ch} for all h are obtained (the minimal values are zero). The minimum of these maximum values of ω_{ch} is calculated to be 0.95 justifying setting ω_{ch} to 1.

TABLE III
MAGNITUDES AND PHASES OF PROPOSED CASCADE PR CONTROLLER AT RESONANT FREQUENCIES

Harmonic order, h	1	3	17	19
Ideal magnitude, K_{Ih}	100	100	100	100
Real magnitude, $M_{\mathrm{PR}h}$	97.1	97.2	100.7	102.0
Magnitude error	−2.9	−2.8	0.7	2.0
Ideal phase, φ_h	5.4°	16.2°	91.8°	102.6°
Real phase, $\varphi_{\mathrm{PR}h}$	5.3°	15.8°	90.9°	102.2°
Phase error	−0.1°	−0.4°	−0.9°	−0.4°

Fig. 2 depicts the frequency responses of proposed cascade PR controllers realized in both *z* domain and *s* domain. As can be seen, they highly overlap indicating the *z*-domain realization method is able to accurately discretize the cascade PR controller, even without a preceding *s*-domain realization.

E. Comparison Between Parallel and Cascade Realization

Fig. 2 displays the frequency responses of an illustrative PR controller implemented using both the parallel method and the proposed cascade method in the s domain. It can be seen that the resonant magnitudes of parallel PR controller exceed K_{Ih}, in low frequency range. In addition, Fig. 2(b) is the zoom-in view of Fig. 2(a) around 19th order harmonic frequency. The parallel PR controller lags cascade PR controller by 8.8° at 19th order harmonic frequency.

For a clearer comparison, Table III lists the expected resonant magnitudes (K_{Ih}) and phase leads (φ_h), and the actual value of the cascade PR controller at selected 1st, 3rd, 17th, and 19th order harmonics to see its characteristics at low frequency and high frequency. In contrast to parallel PR controller (see Table II) where magnitude error is as high as 15.2, the magnitude errors of cascade realization are at most −2.9. Regarding phase lead, the cascade realization manages to restrict phase error within ± 1° (see Table III) much smaller than the 9.2° error of parallel PR controller (see Table II).

Phase lag in high frequency range is unfavorable to stability. This can be verified by Fig. 9 showcasing the Nyquist plots of open loop transfer functions, i.e.,

$$G_{\mathrm{o}}(s) = P(s)G_{\mathrm{PR}}(s) \tag{29}$$

with different PR controllers. In Fig. 9(a), the conventional parallel PR controller is used with no phase compensation. The system is stable with a highest order, h, of 11 (solid blue line), whereas it becomes unstable with h reaching 13, when the Nyquist curve (red dashed line) encompasses the point,

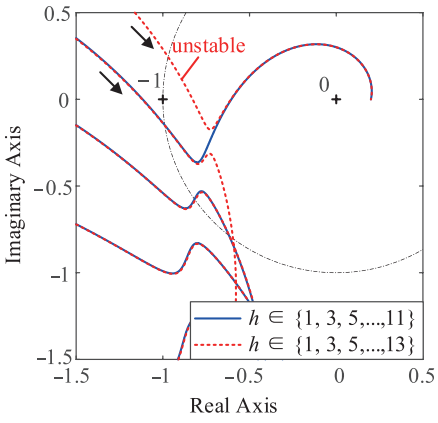

(a)

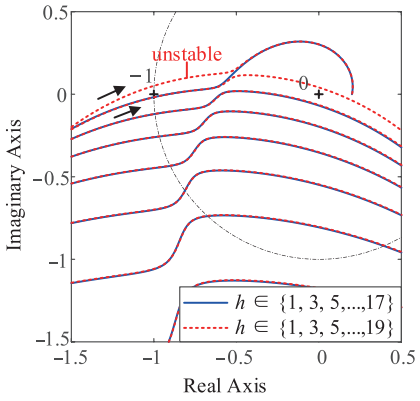

(b)

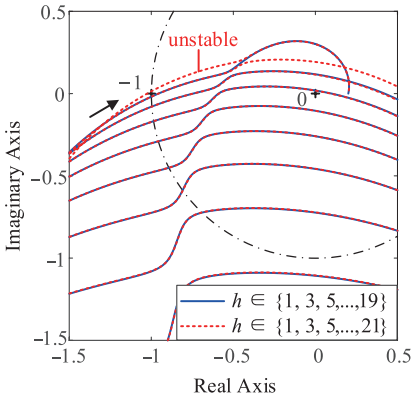

(c)

Fig. 9. Nyquist plots of open loop transfer functions using (a) parallel PR controllers with no phase lead, (b) parallel PR controller with phase lead, and (c) cascade PR controller with phase lead. K_{1h} is set to 100 for all h. other parameters are listed in Table I.

−1. For comparison, Fig. 9(b) shows the Nyquist plots of the open loop transfer function using parallel PR controller with compensation angle. The stability is significantly enhanced. The system is stable with PR controller tuned at up to 17th order harmonic, but unstable with 19th order harmonic. Further, when cascade PR controller with compensation angle is used (see Fig. 9(c)), the system can be stabilized with PR controller tuned at up to 19th order harmonic.

TABLE IV
HIGHEST ORDER OF HARMONICS THE PR CONTROLLER CAN BE TUNED AT UNDER DIFFERENT K_{1h} AND DIFFERENT REALIZATION METHODS

K_{1h}	PR without phase lead	PR with phase lead	
		Parallel	Cascade
100	11	17	19
180	11	15	17
250	11	15	15

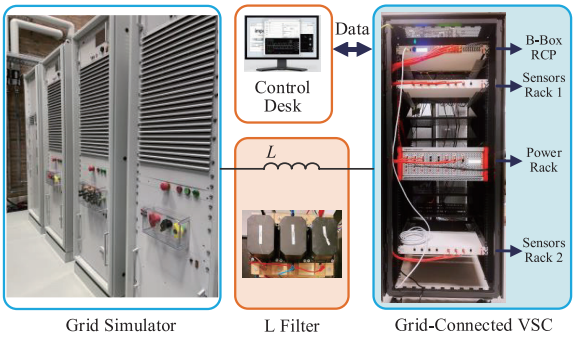

Fig. 10. A down-scaled single-phase grid-tied converter with an L filter.

Table IV summarizes the highest order of harmonics different PR controllers can be tuned at while stabilizing the system of Fig. 1. Other parameters are listed in Table I. As can be seen, the highest order is related to two major factors, phase lead and integral gain. From a vertical view, the highest order the PR controller can be tuned at decreases as integral gain increases. From a horizontal view, a PR controller with phase lead can stabilize in a higher order than that without phase lead, justifying that phase lead can greatly increase stable margin. Moreover, cascade PR controller stabilizes the system with higher order harmonics than parallel PR controller because of more accurate phase lead.

IV. EXPERIMENTAL VERIFICATION

To further verify the theoretical analysis, experiments are carried out on a single-phase grid-tied converter with an L filter, as shown in Fig. 10. The grid is emulated with a high-fidelity linear amplifier APS 15000. The applied half bridge module and the control platform are a PEB-SiC-8024 module and a B-BOX RCP control platform from Imperix, respectively. Sampling frequency and switching frequency are set to the same value of 5 kHz. Other relevant system parameters of the single-phase grid-tied converter with L-Filter is presented in Table I.

A. Stability Verification

To illustrate the harmonic resisting ability of multi-resonance PR controller, grid voltage is added with 10% 3rd, 10% 9th and 10% 15th order harmonics. In experiment, DC link connects to only a capacitor without a DC voltage source. Thus, *d*-axis current reference is given by a DC voltage regulator to maintain a constant DC-link voltage. In steady state, the *d*-axis

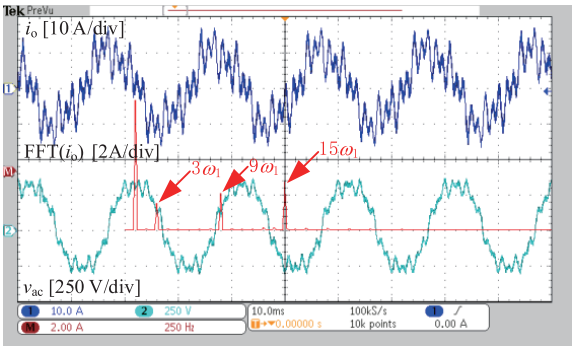

Fig. 11. Waveforms of grid voltage and grid current with parallel PR controller tuned at only fundamental frequencies. Grid voltage contains 10% 3rd, 10% 9th, and 10% 15th order harmonic components.

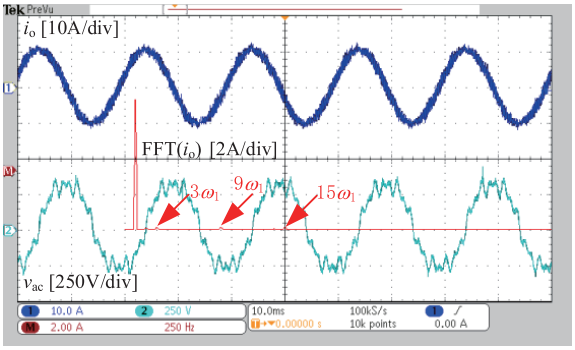

(a)

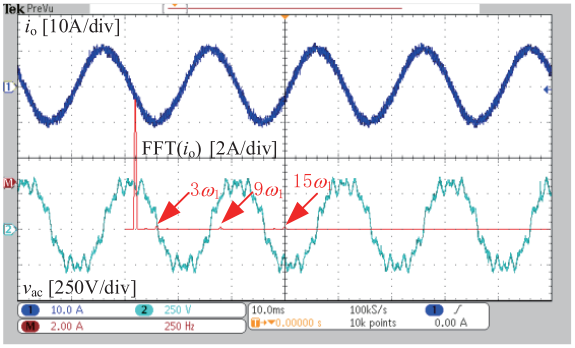

(b)

Fig. 12. Waveforms of grid voltage and grid current with (a) parallel PR controller and (b) cascade PR controller tuned at up to 15th harmonics. Grid voltage contains 10% 3rd, 10% 9th, and 10% 15th order harmonic components.

current is negligible. Meanwhile, the q-axis current reference, I^*, is set to constant 10 A. K_{Ih} for R controllers is set to 180 for all h.

Fig. 11 shows the experimental result when a parallel PR controller tuned at only fundamental frequency is used. As can be seen, the output current is distorted heavily since no R controller tuned at harmonic frequencies is added. The FFT analysis conducted by the oscilloscope indicates that the magnitudes of 3rd, 9th, and 15th order harmonic components are about 1.6 A, 2 A and 2.8 A in RMS, respectively.

Fig. 12 shows the experimental results with either a

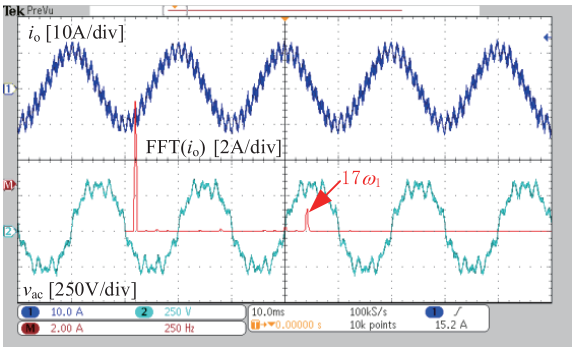

(a)

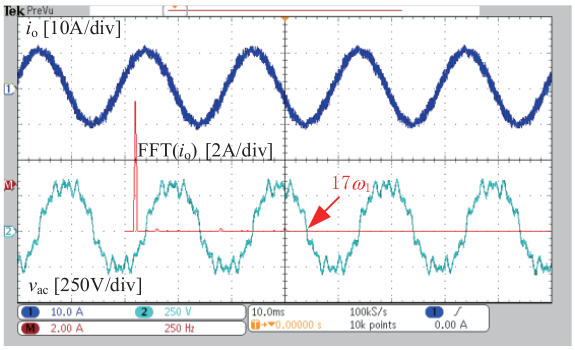

(b)

Fig. 13. Waveforms of grid voltage and grid current with (a) parallel PR controller and (b) cascade PR controller tuned at up to 17th harmonics.

parallel PR controller (Fig. 12 (a)) or a cascade PR controller (Fig. 12 (b)) implemented. Both PR controllers are tuned at all odd order harmonics up to 15th order. As it can be seen, both controllers can stabilize the system in consistency with Table IV. Besides, the output currents contain less harmonics compared with Fig. 11. Regarding their FFT analysis, the 3rd, 9th, and 15th order harmonic components are significantly reduced and can be neglected. This is because R controllers tuned at harmonics are added.

Further, Fig. 13 shows waveforms with the same setup as Fig. 12 except that an additional R controller tuned at 17th order harmonic is added to the PR controllers. It is obvious that the output current of the parallel PR controller (see Fig. 13(a)) contains an amount of 17th order harmonic. Whereas the output current of the cascade PR controller (see Fig. 13(b)) is rather sinusoidal with a negligible amount of harmonics. These are consistent with Table IV, that the parallel PR controller is unstable when tuned at 17th harmonic with a K_{Ih} of 180, whereas the cascade PR controller is stable. It proves that the phase lag caused by inaccurate realization of parallel form jeopardizes the stability of the system.

B. Performance Under Frequency Deviation

This subsection investigates the PR controller's harmonic-resisting ability with deviated fundamental frequency. The transfer function from grid voltage, v_{ac}, to output current, i_o, is derived as:

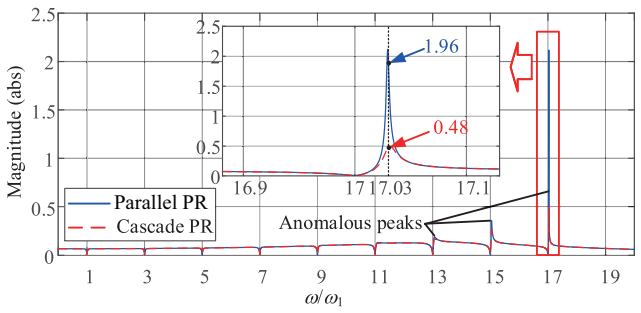

Fig. 14. Magnitude curves of $G_v(s)$ with parallel and cascade PR controllers.

$$G_v(s) = \frac{i_o(s)}{v_{ac}(s)} = -\frac{\frac{1}{sL+R}}{1+P(s)G_{PR}(s)} \tag{30}$$

Fig. 14 presents the magnitude curves of (30) with cascade and parallel PR controllers. K_{ih} is set to 100 for all h. As can be seen, anomalous peaks appear around resonant frequencies [17], specifically 13th, 15th, and 17th order harmonics, indicating a larger current error will result from the corresponding frequency component of grid voltage. Nonetheless, the system with parallel PR controller always gives a larger anomalous peak compared with cascade PR controller, because of larger phase lag [17]. The comparison is stark from the zoom-in view around 17th harmonic. At 17.03 per unit, or 851.53 Hz, the magnitudes of $G_v(s)$ with parallel PR controller is 1.96 much larger than that of cascade PR controller, which is 0.48.

To validate this comparison, relevant experiments were conducted. A 5% 17th harmonic was introduced into the grid voltage, with a fundamental frequency set to 50.09 Hz. Consequently, the corresponding 17th harmonic frequency was 851.53 Hz (17.03 per unit). Fig. 15 presents the experimental results for both cascade and parallel PR controllers. The current reference was set to zero to exclusively highlight the influence of the 17th order voltage harmonic. Upon conducting FFT analysis, it is evident that the harmonic current with the parallel PR controller is approximately 6 A in RMS, almost three times the harmonic current observed with the cascade PR controller, which is approximately 2.2 A in RMS. Note that the results may not be in strict quantitative alignment with Fig. 14, potentially due to challenges in precisely locating sharp anomalous peaks with the finite accuracy of the equipment used. Nevertheless, the outcome in Fig. 15 conclusively validates that the cascade PR controller exhibits smaller anomalous peaks compared to the parallel PR controller.

V. Conclusion

This paper proposes a cascade realization method for PR controllers to cope with the frequency characteristics error at resonant frequencies caused by small integral gain. Firstly, through pole-zero map analysis, the resonant decoupling property of the PR controller has been formulated, which enables PRUs to be designed or realized separately. Pole-zero placement method is used to realize PRU by mapping all

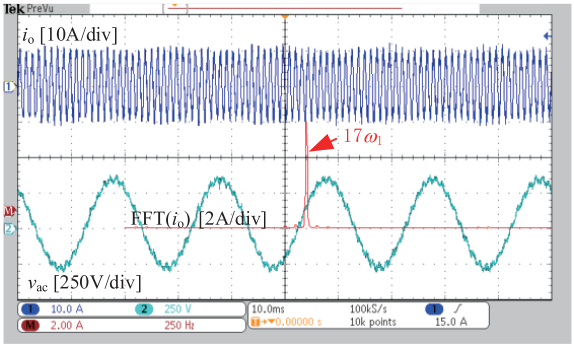

(a)

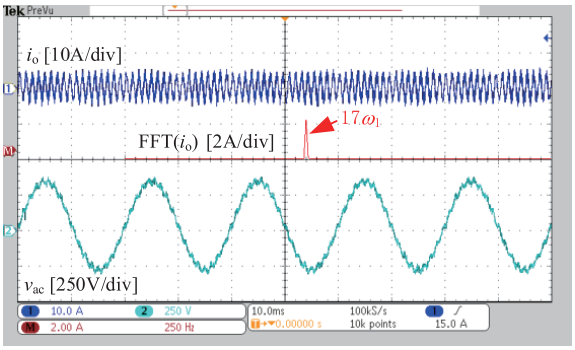

(b)

Fig. 15. Waveforms of grid voltage and grid current with (a) parallel PR controller and (b) cascade PR controller tuned at up to 17th order harmonics. Grid fundamental frequency is set to 50.09 Hz. 5% 17th order harmonic is added to the grid voltage.

parameters of the PR controller to the locations of the pole and zero of the PRU. The difference between a zero and its paired pole is restricted to restrict the frequency characteristics error. The proposed cascade realization is comprehensively compared with traditional parallel realization. It is found that cascade form realizes PR controller with much smaller magnitude and phase error than parallel form. Thus, cascade form can stabilize the system with R controller tuned at higher order compared to parallel form. Relevant experiments verify the correctness of the theoretical analysis and show the superiority of cascade realization.

References

[1] W. Ding, L. Ming, C. Yin, M. Chen, and P. C. Loh, "Differential-mode filters with common-mode neutral-point-balancing accelerators for single-phase symmetrical five-level converters," in *IEEE Transactions on Power Electronics*, vol. 36, no. 8, pp. 9209–9220, Aug. 2021.

[2] D. N. Zmood and D. G. Holmes, "Stationary frame current regulation of PWM inverters with zero steady-state error," in *IEEE Transactions on Power Electronics*, vol. 18, no. 3, pp. 814–822, May 2003.

[3] C. Gong, W. K. Sou, and C. S. Lam, "Design and analysis of vector proportional-integral current controller for LC-coupling hybrid active power filter with minimum DC-link voltage," in *IEEE Transactions on Power Electronics*, vol. 36, no. 8, pp. 9041–9056, Aug. 2021.

[4] W. Ding, L. Ming, C. Yin, P. C. Loh, B. Duan, and C. Zhang, "An integrated common-mode fast-balancing mechanism for three-phase three-level converter with LCL filter," in *IEEE Transactions on Power Electronics*, vol. 36, no. 11, pp. 12694–12709, Nov. 2021.

[5] Z. Li, Y. Li, P. Wang, H. Zhu, C. Liu, and F. Gao, "Single-loop digital

control of high-power 400-Hz ground power unit for airplanes," in *IEEE Transactions on Industrial Electronics*, vol. 57, no. 2, pp. 532–543, Feb. 2010.

[6] M. Elkayam and A. Kuperman, "Optimized design of multiresonant AC current regulators for single-phase grid-connected photovoltaic inverters," in *IEEE Journal of Photovoltaics*, vol. 9, no. 6, pp. 1815–1818, Nov. 2019.

[7] L. Antonio De Souza Ribeiro, F. D. Freijedo, F. De Bosio, M. Soares Lima, J. M. Guerrero, and M. Pastorelli, "Full discrete modeling, controller design, and sensitivity analysis for high-performance grid-forming converters in islanded microgrids," in *IEEE Transactions on Industry Applications*, vol. 54, no. 6, pp. 6267–6278, Nov. 2018.

[8] R. Teodorescu, F. Blaabjerg, M. Liserre, and P. C. Loh, "Proportional-resonant controllers and filters for grid-connected voltage-source converters," in *IEE Proceedings: Electric Power Applications*, vol. 153, no. 5, pp. 750–762, Sept. 2006.

[9] Z. Xin, P. C. Loh, X. Wang, F. Blaabjerg, and Y. Tang, "Highly accurate derivatives for LCL-filtered grid converter with capacitor voltage active damping," in *IEEE Transactions on Power Electronics*, vol. 31, no. 5, pp. 3612–3625, May 2016.

[10] R. I. Bojoi, G. Griva, V. Bostan, M. Guerriero, F. Farina, and F. Profumo, "Current control strategy for power conditioners using sinusoidal signal integrators in synchronous reference frame," in *IEEE Transactions on Power Electronics*, vol. 20, no. 6, pp. 1402–1412, Nov. 2005.

[11] B. Xie, K. Guo, M. Mao, L. Zhou, T. Liu, Q. Zhang, and G. Hao, "Analysis and improved design of phase compensated proportional resonant controllers for grid-connected inverters in weak grid," in *IEEE Transactions on Energy Conversion*, vol. 35, no. 3, pp. 1453–1464, Sept. 2020.

[12] F. González-Espín, I. Patrao, E. Figueres, and G. Garcerá, "An adaptive digital control technique for improved performance of grid connected inverters," in *IEEE Transactions on Industrial Informatics*, vol. 9, no. 2, pp. 708–718, May 2013.

[13] P. C. Loh, D. M. Vilathgamuwa, S. K. Tang, and H. L. Long, "Multilevel dynamic voltage restorer," in *IEEE Power Electronics Letters*, vol. 2, no. 4, pp. 125–130, Dec. 2004.

[14] D. N. Zmood, D. G. Holmes, and G. H. Bode, "Frequency-domain analysis of three-phase linear current regulators," in *IEEE Transactions on Industry Applications*, vol. 37, no. 2, pp. 601–610, Mar. 2001.

[15] S. Zhou and J. Liu, "Analysis and comparison of resonant-based current controllers implemented in stationary reference frame: A complex pole-zero placement perspective," in *Proceedings of 2015 IEEE Energy Conversion Congress and Exposition (ECCE)*, Montreal, QC, Canada, 2015, pp. 1624–1631.

[16] M. Castilla, J. Miret, J. Matas, L. G. de Vicuña, and J. M. Guerrero, "Control design guidelines for single-phase grid-connected photovoltaic inverters with damped resonant harmonic compensators," in *IEEE Transactions on Industrial Electronics*, vol. 56, no. 11, pp. 4492–4501, Nov. 2009.

[17] A. G. Yepes, F. D. Freijedo, Ó. López, and J. Doval-Gandoy, "Analysis and design of resonant current controllers for voltage-source converters by means of nyquist diagrams and sensitivity function," in *IEEE Transactions on Industrial Electronics*, vol. 58, no. 11, pp. 5231–5250, Nov. 2011.

[18] A. G. Yepes, F. D. Freijedo, Ó. López, and J. Doval-Gandoy, "High-performance digital resonant controllers implemented with two integrators," in *IEEE Transactions on Power Electronics*, vol. 26, no. 2, pp. 563–576, Feb. 2011.

[19] C. Tang, K. Zhou, Y. Shu, Q. He, and Q. Chen, "Analysis and design of multiple resonant current control for grid-connected converters," in *IEEE Journal of Emerging and Selected Topics in Power Electronics*, vol. 10, no. 2, pp. 2539–2546, Apr. 2022.

[20] B. Lin, L. Peng, and X. Liu, "Selective pole placement and cancellation for proportional-resonant control design used in voltage source inverter," in *IEEE Transactions on Power Electronics*, vol. 37, no. 8, pp. 8921–8934, Aug. 2022.

[21] C. Lascu, L. Asiminoaei, I. Boldea, and F. Blaabjerg, "Frequency response analysis of current controllers for selective harmonic compensation in active power filters," in *IEEE Transactions on Industrial Electronics*, vol. 56, no. 2, pp. 337–347, Feb. 2009.

[22] C. Lascu, L. Asiminoaei, I. Boldea, and F. Blaabjerg, "High performance current controller for selective harmonic compensation in active power filters," in *IEEE Transactions on Power Electronics*, vol. 22, no. 5, pp. 1826–1835, Sept. 2007.

[23] H. Bai, X. Wang, P. C. Loh, and F. Blaabjerg, "An active trap filter for switching harmonic attenuation of low-pulse-ratio inverters," in *IEEE Transactions on Power Electronics*, vol. 32, no. 12, pp. 9078–9092, Dec. 2017.

[24] C. Xia, B. Ji, and Y. Yan, "Smooth speed control for low-speed high-torque permanent-magnet synchronous motor using proportional-integral-resonant controller," in *IEEE Transactions on Industrial Electronics*, vol. 62, no. 4, pp. 2123–2134, Apr. 2015.

[25] C. Xie, X. Zhao, K. Li, J. Zou, and J. M. Guerrero, "A new tuning method of multiresonant current controllers for grid-connected voltage source converters," in *IEEE Journal of Emerging and Selected Topics in Power Electronics*, vol. 7, no. 1, pp. 458–466, Mar. 2019.

[26] F. Hans, W. Schumacher, S. F. Chou, and X. Wang, "Design of multi-frequency proportional-resonant current controllers for voltage-source converters," in *IEEE Transactions on Power Electronics*, vol. 35, no. 12, pp. 13573–13589, Dec. 2020.

[27] C. A. Busada, S. Gómez Jorge, A. E. Leon, and J. A. Solsona, "Current controller based on reduced order generalized integrators for distributed generation systems," in *IEEE Transactions on Industrial Electronics*, vol. 59, no. 7, pp. 2898–2909, Jul. 2012.

Chao Gao received the B.S. degree from Wuhan University, Wuhan, China, in 2018, and the M.S. degree from Huazhong University of Science and Technology, Wuhan, China, in 2021, both in electrical engineering. He is currently working toward the Ph.D. degree from the Chinese University of Hong Kong, Hong Kong, China. His research interests include modeling and control of power electronic converters.

Shuyu Zhang received her B.Eng. degree in Electrical Engineering from Huazhong University of Science and Technology, Wuhan, China, in 2023. She is currently pursuing a Master's degree in Electrical Engineering at Stanford University. Her research focuses on multilevel converters and the study of electromagnetic interference in Power Electronic Systems.

Bo Lu received the B.S. and M.S. degrees from Huazhong University of Science and Technology, Wuhan, China, in 2018 and 2021, respectively, both in electrical engineering. He is currently working toward the Ph.D. degree from Fudan University, Shanghai, China. His research interests include high-precision and high-efficient power amplifiers.

Wenlong Ding received the B.S. and M.S. degrees from Qufu Normal University, Rizhao, China, in 2011 and 2014, respectively, and the Ph.D. degree from Shandong University, Jinan, China, in 2019, all in electrical engineering. From November 2019 to August 2020, he was a Post-Doctoral Research Fellow with the Department of Electronic Engineering, The Chinese University of Hong Kong, Hong Kong, China. He was with the Hong Kong Applied Science and Technology Research Institute (ASTRI), Hong Kong, from September 2020 to November 2021. Since 2021, he has been with the School of Control Science and Engineering, Shandong University. His current research interests include applications of wide band gap (WBG) devices, multilevel converters, and battery charging/testing technology.

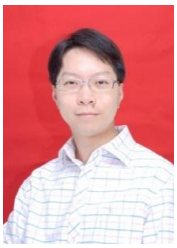

Ka Nang Leung received the B.Eng., M.Phil., and Ph.D. degrees in Electrical and Electronic Engineering from Hong Kong University of Science and Technology (HKUST), Clear Water Bay, Hong Kong, in 1996, 1998, and 2002, respectively. In 2002, he was a Visiting Assistant Professor at HKUST. In 2005, he joined with the Department of Electronic Engineering, Chinese University of Hong Kong, Hong Kong, where he is currently an Associate Professor. His research interests include power-management integrated circuits and low-voltage low-power analog integrated circuits.

Dr. Leung is the Chairman of the IEEE (Hong Kong) Electron Device/ Solid-State Circuit Joint Chapter in 2012. He is a member in the Editorial Boards and a guest editor of a special issue of Energies. He serves as a Paper Reviewer in numerous IEEE journals and IEEE international conferences. Moreover, he is actively involved in the organization of IEEE international conferences. He is a co-recipient of the Best Paper Awards of TENCON in 2015 and the IEEE Student Symposium ED/SSC in 2011, 2014 and 2019.

Poh Chiang Loh received the B.Eng. (hons.) and M.Eng. degrees from the National University of Singapore, Singapore, in 1998 and 2000, respectively, and the Ph.D. degree from Monash University, Melbourne, Vic, Australia, in 2002, all in electrical engineering.

From 2013 to 2015, he was a Professor with Aalborg University, Aalborg, Denmark. Since 2015, he has been a Tenured Full Professor with the Chinese University of Hong Kong, Hong Kong, China. His research interests include power converters and their grid applications.